Exact stationary solutions for the translationally invariant discrete nonlinear Schrödinger equations

2007 J. Phys. A: Math. Theor. 40 1727

(http://iopscience.iop.org/1751-8121/40/8/003)

IOP PUBLISHING JOURNAL OF PHYSICS A: MATHEMATICAL AND THEORETICAL

J. Phys. A: Math. Theor. **40** (2007) 1727–1746 doi:10.1088/1751-8113/40/8/003

Exact stationary solutions for the translationally invariant discrete nonlinear Schrödinger equations

S V Dmitriev[1], P G Kevrekidis[2], N Yoshikawa[1] and D J Frantzeskakis[3]

[1] Institute of Industrial Science, University of Tokyo, 4-6-1 Komaba, Meguro-ku, Tokyo 153-8505, Japan
[2] Department of Mathematics and Statistics, University of Massachusetts Lederle Graduate Research Tower, Amherst, MA 01003-4515, USA
[3] Department of Physics, University of Athens, Panepistimiopolis, Zografos, Athens 15784, Greece

Received 25 October 2006, in final form 5 January 2007
Published 6 February 2007
Online at stacks.iop.org/JPhysA/40/1727

Abstract

From a wide class of translationally invariant discrete nonlinear Schrödinger (DNLS) equations, we extract a two-parameter subclass corresponding to Kerr nonlinearity for which *any* stationary solution can be derived recurrently from a quadratic equation. This subclass, which incorporates the integrable (Ablowitz–Ladik) lattice as a special case, admits exact stationary solutions that are derived in terms of the Jacobi elliptic functions. Exact moving solutions for the discrete equations are also obtained. In the continuum limit, the constructed stationary solutions reduce to the exact moving solutions to the continuum NLS equation with Kerr nonlinearity. Numerical results are also presented for the special case of localized solutions, including sech (pulse, or bright soliton), tanh (kink, or dark soliton) and 1/tanh (called here inverted kink) profiles. For these solutions, we discuss their linearization spectra and their mobility. Particularly, we demonstrate that discrete dark solitons are dynamically *stable* for a wide range of lattice spacings, contrary to what is the case for their standard DNLS counterparts. Furthermore, the bright and dark solitons in the non-integrable, translationally invariant lattices can propagate at slow speed without any noticeable radiation.

PACS numbers: 03.40.Kf, 63.20.Pw

Dedicated to the memory of collaborator and friend Shozo Takeno

1. Introduction

In continuum nonlinear equations without external spatially dependent potentials, the existing solitary wave solutions are invariant with respect to a shift along the spatial coordinate due to the so-called translational invariance. In lattice equations translational invariance is usually

lost and the static/stationary solutions exist only for a discrete set of positions with respect to the lattice. Generally speaking, discreteness also limits the mobility of localized structures, but this is not always the case. For instance, there exist (a few) integrable lattices where the coherent structures can be placed anywhere with respect to the lattice and can propagate without any energy loss [1–3].

On the other hand, a class of *non-integrable*, translationally invariant (TI) Klein–Gordon lattices was recently developed. Relevant theoretical studies first appeared in the pioneering works [4–6], and then generalized on the basis of the discretized first integral (DFI) approach in [7, 8] (see also the concurrent works of [9, 10] for a slightly different perspective). Other contributions to this problem [11–14] are devoted to additional related models and their properties, such as collisions of the solitary waves. On the other hand, looking for the stationary, standing wave solutions of the continuum nonlinear Schrödinger (NLS) equation with general nonlinearity reduces the problem to the corresponding continuum Klein–Gordon equation. Thus, the DFI method of constructing the TI discretizations developed for the Klein–Gordon equation can be immediately applied to the NLS one [15, 16].

The TI discretizations are important from both a mathematical and a physical standpoint since they provide discrete models whose coherent structures are not 'trapped' by the lattice, even in the highly discrete regime. For typical discretizations, given that solutions can be found only for a discrete set of positions with respect to the lattice (typically on a lattice site and at the middle between two adjacent lattice sites), a potential barrier (the so-called Peierls–Nabarro barrier) needs to be overcome in order to observe wave propagation over the lattice. However, for TI discretizations, since such a barrier is absent, it is easier for waves to propagate without radiation losses or to be accelerated by even weak external fields. In that respect, the TI models emulate more closely their continuum siblings rather than their non-TI counterparts. Furthermore, occasionally, they may constitute the proper physical model in their own right [12]. For these and related reasons, the TI discrete nonlinear Schrödinger (DNLS) equations have been recently receiving considerable attention [15–19]. A review and classification of various TI DNLS models can be found in the very recent work of [19]. Some of the DNLS models with cubic (Kerr) nonlinearity support exact stationary solutions that can be expressed in terms of the Jacobi elliptic functions [17, 18]. Similar solutions have been reported for the ϕ^4 TI lattices [8, 11], and it was demonstrated that the full set of the stationary solutions can be derived from the corresponding DFI [8]. The Jacobi elliptic function solutions were found for the models whose DFI is a quadratic algebraic equation. Although this technique cannot be used for DFIs of arbitrary order, it is still worthwhile to obtain such solutions due to the physical relevance of the underlying cubic nonlinear models. An alternative but equally compelling motivation is that these belong to a special group, consisting of very few nonlinear models (especially non-integrable ones), where the families of stationary solutions can be obtained in closed form.

For the above reasons, in the present study, from a wide class of the TI DNLS models with Kerr nonlinearity constructed in [15, 16], we extract a two-parameter subclass whose DFI is a quadratic algebraic equation. Then, we present a set of stationary Jacobi elliptic function solutions to this DNLS model and, following the approach presented in [8], we also demonstrate how to derive all possible stationary solutions iteratively from the DFI. Examples of the exact lattice solutions moving with a selected velocity are also given. In the continuum limit, the constructed Jacobi elliptic function solutions transform to the full set of moving solutions of the continuum NLS model with focusing and defocusing Kerr nonlinearities, including possible unbounded ones.

Our presentation is structured as follows. In section 2, we present the general setup of the continuum NLS equation with Kerr nonlinearity and its two-parameter discrete, TI model.

Conservation laws supported by different subclasses of the considered model are discussed in section 3. Exact stationary solutions for the lattice equations are given in section 4 and the exact moving solutions in section 5. A numerical study of the stability and other related properties for the selected group of hyperbolic function solutions is carried out in section 6. The full set of the exact moving solutions of the continuum NLSE with Kerr nonlinearity is obtained in section 7. Finally, in section 8, we briefly summarize our findings and present our conclusions.

2. Setup

We start our study considering the NLS equation with Kerr nonlinearity, expressed in the following dimensionless form:

$$\mathrm{i}\psi_t + \tfrac{1}{2}\psi_{xx} + \lambda|\psi|^2\psi = 0, \tag{1}$$

where the parameter $\lambda = \pm 1$ (the cases $\lambda = +1$ or $\lambda = -1$ correspond to a focusing or a defocusing nonlinearity, respectively).

Seeking stationary solutions of equation (1) in the form

$$\psi(x,t) = f(x)\,\mathrm{e}^{\mathrm{i}\omega t}, \tag{2}$$

we reduce the NLS equation to an ordinary differential equation (ODE) for the real function $f(x)$,

$$D(x) \equiv f'' - 2\omega f + 2\lambda f^3 = 0. \tag{3}$$

The latter ODE has the form of an equation of motion of a one-dimensional dynamical system, which possesses the first integral

$$u(x) \equiv (f')^2 - 2\omega f^2 + \lambda f^4 + C = 0, \tag{4}$$

where C is the integration constant, representing the total energy of the above dynamical system.

We introduce the lattice $x_n = nh$, where h is the lattice spacing and $n = 0, \pm 1, \pm 2, \ldots$. For convenience, we also introduce the following shorthand notations:

$$f(x_{n-1}) = f_-, \qquad f(x_n) = f_n, \qquad f(x_{n+1}) = f_+, \tag{5}$$

and will focus only on discretizations that involve such nearest neighbour sites.

We then involve the following two-point discretization of the first integral equation (4),

$$u(f_-, f_n) \equiv \frac{1}{h^2}(f_n - f_-)^2 - 2\omega f_- f_n + \lambda f_-^2 f_n^2 + C = 0. \tag{6}$$

In principle, it is possible to construct a more general discretization of equation (4) involving also terms cubic and quartic in f_n [15, 16]. However, here we retain only quadratic terms, which, as we will show below, allows for a straightforward determination of the solutions in terms of the Jacobi elliptic functions.

Discretizing the left-hand side of the identity $(1/2)\,\mathrm{d}u/\mathrm{d}f = D(x)$, we obtain the discrete version of equation (3),

$$\begin{aligned} D(f_-, f_n, f_+) &\equiv \frac{u(f_n, f_+) - u(f_-, f_n)}{f_+ - f_-} \\ &= \frac{f_- - 2f_n + f_+}{2h^2} - \omega f_n + \frac{\lambda}{2}(f_- + f_+) f_n^2 = 0. \end{aligned} \tag{7}$$

Formally, $D(f_-, f_n, f_+) = 0$ is a three-point problem but, clearly, its solutions can be found from the two-point problem $u(f_-, f_n) = 0$, equation (6), which is a quadratic algebraic equation.

The TI discretization of equation (1) reads

$$\mathrm{i}\dot{\psi}_n + \frac{1}{2h^2}(\psi_- - 2\psi_n + \psi_+) + \frac{\lambda}{2}S(\psi_-, \psi_n, \psi_+) = 0, \tag{8}$$

where the overdot denotes time derivative, and $S(\psi_-, \psi_n, \psi_+)$ is any function that, upon substituting

$$\psi_n(t) = f_n\,\mathrm{e}^{\mathrm{i}\omega t}, \tag{9}$$

reduces to $(f_- + f_+)f_n^2\,\mathrm{e}^{i\omega t}$. For example, the following two-parameter DNLS equation can be offered:

$$\mathrm{i}\dot{\psi}_n + \frac{1}{2h^2}(\psi_- - 2\psi_n + \psi_+) + \frac{\lambda}{2}\big\{\delta_1\psi_n(|\psi_-\psi_n| + |\psi_n\psi_+|) + \delta_2(\psi_- + \psi_+)|\psi_n|^2 + \delta_3(\psi_-^\star + \psi_+^\star)\psi_n^2\big\} = 0, \tag{10}$$

with the coefficients satisfying the continuity constraint,

$$\delta_1 + \delta_2 + \delta_3 = 1. \tag{11}$$

We note in passing that the δ_1 term of equation (10) was not discussed in the work [19] where a ten-parameter DNLS model was investigated.

Stationary solutions to equation (10) of the form of equation (9) can be found from the two-point nonlinear map equation (6), which we rewrite in the form of

$$(f_n - f_-)^2 + 2(1 - \Omega)f_-f_n + \Lambda f_-^2 f_n^2 + S = 0, \tag{12}$$

where

$$\Omega = 1 + \omega h^2, \qquad \Lambda = \lambda h^2, \qquad S = Ch^2. \tag{13}$$

3. Conservation laws

The two-parameter TI DNLS model of equation (10) contains subclasses conserving the classical norm

$$N = \sum_n |\psi_n|^2, \tag{14}$$

the modified norm

$$\tilde{N} = \frac{1}{2}\sum_{n=-\infty}^{\infty}(\psi_n\psi_+^\star + \psi_n^\star\psi_+), \tag{15}$$

and the classical momentum

$$P = \mathrm{i}\sum_{n=-\infty}^{\infty}(\psi_n\psi_+^\star - \psi_n^\star\psi_+). \tag{16}$$

The above-conserved quantities are illustrated in figure 1 on the (δ_1, δ_2) plane.

To demonstrate that these quantities are indeed conserved, we first calculate the time derivatives $\mathrm{d}N/\mathrm{d}t$, $\mathrm{d}\tilde{N}/\mathrm{d}t$, and $\mathrm{d}P/\mathrm{d}t$, and then substitute in these expressions $\mathrm{i}\dot{\psi}_n$ using equation (10). This way, we come to the following results:

$$\frac{\mathrm{d}N}{\mathrm{d}t} = \lambda(\delta_2 - \delta_3)\sum_n |\psi_n|^2[I_n(R_- + R_+) - R_n(I_- + I_+)], \tag{17}$$

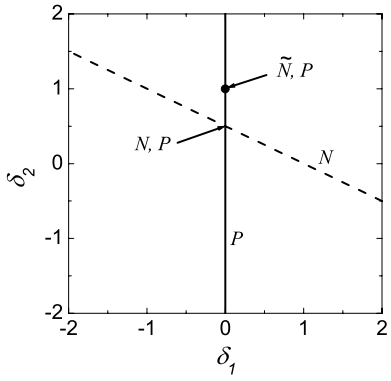

Figure 1. Conserved quantities for the TI DNLS model of equation (10) shown on the (δ_1, δ_2) plane. The norm N is conserved on the dashed line $\delta_2 = (1 - \delta_1)/2$. The modified norm $\tilde{N}$ is conserved at the point $(\delta_1, \delta_2) = (0, 1)$, which corresponds to the integrable discretization. The momentum P is conserved on the solid line $\delta_1 = 0$. Apparently, there is no choice leading to a model that conserves all three quantities simultaneously. Note that N and P are conserved at $(\delta_1, \delta_2) = (0, 1/2)$, while $\tilde{N}$ and P are conserved at $(\delta_1, \delta_2) = (0, 1)$.

$$\frac{\mathrm{d}\tilde{N}}{\mathrm{d}t} = \frac{\lambda}{2}\sum_n (R_n I_+ - R_+ I_n)[\delta_1 |\psi_- \psi_n| + 2\delta_3 (R_- R_n + I_- I_n)]$$
$$+ \frac{\lambda}{2}\sum_n (R_n I_- - R_- I_n)[\delta_1 |\psi_n \psi_+| + 2\delta_3 (R_n R_+ + I_n I_+)], \tag{18}$$

$$\frac{\mathrm{d}P}{\mathrm{d}t} = \lambda\delta_1 \sum_n |\psi_n|(|\psi_-| + |\psi_+|)[R_n(R_- - R_+) + I_n(I_- - I_+)], \tag{19}$$

where we have used the notation

$$R_n = \mathrm{Re}(\psi_n), \qquad I_n = \mathrm{Im}(\psi_n). \tag{20}$$

From equation (17) it is clear that the norm N is conserved ($\mathrm{d}N/\mathrm{d}t = 0$) for arbitrary δ_1 and $\delta_2 = \delta_3$, which, with the use of the continuity constraint of equation (11), corresponds to the dashed line $\delta_2 = (1 - \delta_1)/2$ in the (δ_1, δ_2)-plane shown in figure 1.

On the other hand, from equation (18) we deduce that the modified norm $\tilde{N}$ is conserved for arbitrary δ_2 and $\delta_1 = \delta_3 = 0$, i.e., at the point $(\delta_1, \delta_2) = (0, 1)$ in figure 1.

Finally, from equation (19) we find that the momentum P is conserved for arbitrary δ_2 and δ_3 and for $\delta_1 = 0$, shown by the solid line $\delta_1 = 0$ in figure 1.

Thus, the TI DNLS model of equation (10) does not possess all three conserved quantities simultaneously. On the other hand, it should be mentioned that N and P are simultaneously conserved at the point $(\delta_1, \delta_2) = (0, 1/2)$, while $\tilde{N}$ and P are simultaneously conserved at the point $(\delta_1, \delta_2) = (0, 1)$, which corresponds to the integrable discretization.

4. Exact stationary solutions

In this section we describe all possible exact stationary solutions to the TI DNLS model of equation (10).

4.1. Solutions from nonlinear map

To find *all* stationary solutions to the TI model of equation (10) having the form of equation (9) we solve equation (12) and find the amplitudes:

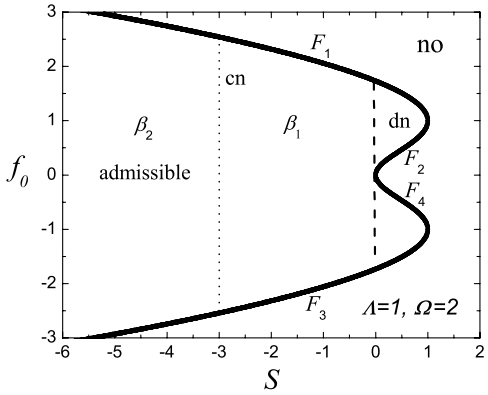

Figure 2. Admissible region for the initial value of f_0 in the nonlinear map equation (21) for different S at $\Lambda = 1$, $\Omega = 2$. Roots F_1 and F_2 merge at $S = (\Omega - 1)^2/\Lambda$, and roots F_2 and F_4 merge at $S = 0$. The dn solution, equation (31), is defined for $0 < S < (\Omega - 1)^2/\Lambda$. The cn solution, equation (30), is defined for $S < 0$, and this region is divided into two parts, β_1 and β_2, each corresponding to a particular root of the first equation in equation (30). The border between these two regions is shown by the dotted line situated (for the chosen parameters) at $S \approx -3.00$.

$$f_n(f_-) = \frac{\Omega f_- \pm \sqrt{\mathcal{D}}}{1 + \Lambda f_-^2}, \tag{21}$$

with

$$\mathcal{D} = \Omega^2 f_-^2 - (1 + \Lambda f_-^2)(S + f_-^2), \tag{22}$$

where f_n and f_- can be interchanged due to the symmetry of equation (12). The solution is obtained by iterating equation (21) and its counterpart written as $f_-(f_n)$, starting from any admissible initial value f_0. Arbitrariness in the choice of the initial condition implies the translational invariance of these models.

As can be seen from equation (21), for fixed Ω, Λ and S, there are certain constraints on the initial value f_0. In particular, there exist inadmissible initial values for which the denominator becomes zero, i.e., $f_0 \neq \pm\sqrt{-1/\Lambda}$ for $\Lambda < 0$, and also ones for which $\mathcal{D} < 0$. The condition $\mathcal{D} = 0$ is a biquadratic algebraic equation providing the borders of the admissible region and has the roots

$$\left(f_0^2\right)_{1,2} = \frac{\Omega^2 - 1 - S\Lambda \pm \sqrt{(\Omega^2 - 1 - S\Lambda)^2 - 4S\Lambda}}{2\Lambda}. \tag{23}$$

We introduce the following notations for these roots:

$$F_1 = -F_3 = \sqrt{\left(f_0^2\right)_1}, \qquad F_2 = -F_4 = \sqrt{\left(f_0^2\right)_2}. \tag{24}$$

The admissible regions are plotted in figures 2 and 3 for $\Lambda = 1$ and $\Lambda = -1$, respectively. The inadmissible regions are marked with 'no'.

Since equation (21) serves for calculating both back and forth points of the map, once started from an admissible value of f_0, one cannot leave the admissible region iterating equation (21), so that the stationary solution will necessarily be constructed for the entire chain.

In the limit of $h \to \infty$, equation (21) is reduced to the following form:

$$f_n = \frac{\omega \pm \sqrt{\omega^2 - \lambda C}}{\lambda f_-}, \tag{25}$$

with inadmissible initial value of $f_0 = 0$ and $\lambda C < \omega^2$.

Solutions in the continuum limit ($h \to 0$) will be presented in section 7.

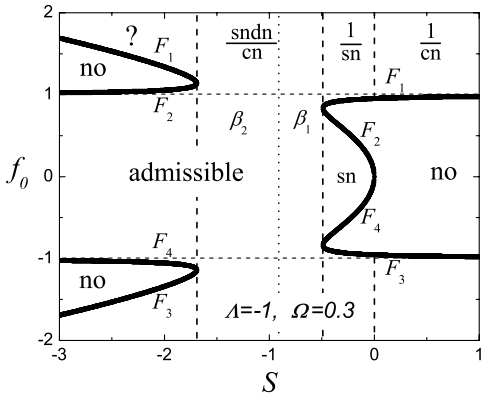

Figure 3. Same as in figure 2 but for $\Lambda = -1$, $\Omega = 0.3$. There are two inadmissible lines, $f_0 \neq \pm\sqrt{-1/\Lambda}$ (horizontal dashed lines), and the three inadmissible regions marked with 'no'. Roots F_1 and F_2 merge at $S = (1 \pm \Omega)^2/\Lambda$, and roots F_2 and F_4 merge at $S = 0$. The 1/cn solution, equation (33), is defined for $S > 0$. The sn solution, equation (29), and the 1/sn solution, equation (32), are defined for $(1 - \Omega)^2/\Lambda < S < 0$. The region of the sndn/cn solution, equation (34), is $(1 + \Omega)^2/\Lambda < S < (1 - \Omega)^2/\Lambda$ and it is divided into two parts corresponding to the roots β_1 and β_2 of the first expression in equation (34); this border is shown by the dotted line situated, for the chosen parameters, at $S \approx -0.91$. We could not find a solution of the form of equation (26) in the region $S < (1 + \Omega)^2/\Lambda$, marked with the question mark (see discussion in the text).

4.2. Jacobi elliptic function solutions

Stationary solutions to equation (10) having the form of equation (9) can also be expressed in terms of the Jacobi elliptic functions (see, e.g. [17, 18]). The amplitude f_n of these solutions is given by the following general expression:

$$\begin{aligned} f_n &= \pm A\,\mathrm{sn}^q(Z,m)\,\mathrm{cn}^r(Z,m)\,\mathrm{dn}^s(Z,m), \\ Z &= \beta h(n + x_0), \end{aligned} \tag{26}$$

where $0 \leqslant m \leqslant 1$ is the modulus of the Jacobi elliptic functions, A and β are the parameters of the solution, x_0 is the arbitrary initial position, and finally the integers q, r, s specify a particular form of the solution.

In the limit of $m = 1$, equation (26) reduces to

$$f_n = \pm A \tanh^q(Z) \cosh^{-r-s}(Z), \tag{27}$$

and, in the limit of $m = 0$, to

$$f_n = \pm A \sin^q(Z) \cos^r(Z). \tag{28}$$

Essentially different, real amplitude solutions of the form of equation (26) are as follows. For $(q, r, s) = (1, 0, 0)$, we have the sn solution with the parameters

$$\Omega = \mathrm{cn}(\beta h)\,\mathrm{dn}(\beta h), \qquad A = \sqrt{\frac{-m}{\Lambda}}\,\mathrm{sn}(\beta h), \qquad S = \frac{1}{m}\Lambda A^4. \tag{29}$$

For $(q, r, s) = (0, 1, 0)$, we have the cn solution with

$$\Omega = \frac{\mathrm{cn}(\beta h)}{\mathrm{dn}^2(\beta h)}, \qquad A = \sqrt{\frac{m}{\Lambda}}\frac{\mathrm{sn}(\beta h)}{\mathrm{dn}(\beta h)}, \qquad S = \frac{m-1}{m}\Lambda A^4. \tag{30}$$

For $(q, r, s) = (0, 0, 1)$, we have the dn solution with

$$\Omega = \frac{\mathrm{dn}(\beta h)}{\mathrm{cn}^2(\beta h)}, \qquad A = \sqrt{\frac{1}{\Lambda}}\frac{\mathrm{sn}(\beta h)}{\mathrm{cn}(\beta h)}, \qquad S = (1-m)\Lambda A^4. \tag{31}$$

For $(q, r, s) = (-1, 0, 0)$, we have the 1/sn solution with

$$\Omega = \mathrm{cn}(\beta h)\,\mathrm{dn}(\beta h), \qquad A = \sqrt{\frac{-1}{\Lambda}}\,\mathrm{sn}(\beta h), \qquad S = m\Lambda A^4. \tag{32}$$

For $(q, r, s) = (0, -1, 0)$, we have the 1/cn solution with

$$\Omega = \frac{\mathrm{cn}(\beta h)}{\mathrm{dn}^2(\beta h)}, \qquad A = \sqrt{\frac{m-1}{\Lambda}}\,\frac{\mathrm{sn}(\beta h)}{\mathrm{dn}(\beta h)}, \qquad S = \frac{m}{m-1}\Lambda A^4. \tag{33}$$

For $(q, r, s) = (1, -1, 1)$, we have the sndn/cn solution with

$$\Omega = \frac{m\mathrm{cn}^4(\beta h) + 1 - m}{\mathrm{cn}^2(\beta h)}, \qquad A = \sqrt{\frac{-1}{\Lambda}}\,\frac{\mathrm{sn}(\beta h)\,\mathrm{dn}(\beta h)}{\mathrm{cn}(\beta h)}, \qquad S = \Lambda A^4. \tag{34}$$

The solutions of equations (30) and (31) have real amplitudes for $\Lambda > 0$ while the others for $\Lambda < 0$. For a given Ω one can find β by solving the first equation in equations (29)–(34), and then A from the second one. Substituting these values into equation (26) we obtain the amplitudes of the stationary solutions of the form of equation (9) that satisfies the discrete NLSE equation (10).

The expressions for S in equations (29)–(34) link the Jacobi elliptic function solutions and the solutions in the form of the nonlinear map of equation (21). As for the other free parameter of the solutions equations (29)–(34), i.e., the arbitrary shift x_0, its counterpart in the nonlinear map, equation (21), is effectively the initial value f_0.

We could not find a solution of the form of equation (26) in the region $S < (1 + \Omega)^2/\Lambda$, marked with the question mark in figure 3. However, this region disappears in the continuum limit (see section 7) and this might be the reason of failure (i.e., solutions may indeed not exist in the considered form for that parametric interval).

5. Exact moving solutions to discrete NLSE

The discrete nonlinear lattice described by equation (10) also supports a number of moving solutions. Here we present only the hyperbolic function solutions that generalize the stationary solutions of equations (54)–(56); nevertheless, similar generalizations of the Jacobi elliptic function solutions equations (29)–(34) can also be obtained.

The moving sech solution (bright soliton) is

$$\begin{aligned} &\psi_n(t) = A\,\mathrm{sech}[\beta h(n + x_0 - vt)]\,\mathrm{e}^{\mathrm{i}(\omega t + \alpha n + \phi_0)}, \\ &\cos\alpha = -\frac{\delta_1}{2\delta_3}, \qquad v = \frac{\sin\alpha\,\sinh(\beta h)}{\beta h^3}, \\ &\Omega = \cos\alpha\,\cosh(\beta h), \qquad A = \frac{\sinh(\beta h)}{\sqrt{\Lambda(\delta_2 - \delta_3)}}. \end{aligned} \tag{35}$$

The moving tanh solution (dark soliton) reads

$$\begin{aligned} &\psi_n(t) = A\tanh[\beta h(n + x_0 - vt)]\,\mathrm{e}^{\mathrm{i}(\omega t + \alpha n + \phi_0)}, \\ &\cos\alpha = -\frac{\delta_1}{2\delta_3}, \qquad v = \frac{\sin\alpha\,\tanh(\beta h)}{\beta h^3}, \\ &\Omega = \cos\alpha\,\mathrm{sech}^2(\beta h), \qquad A = \frac{\tanh(\beta h)}{\sqrt{\Lambda(\delta_3 - \delta_2)}}, \end{aligned} \tag{36}$$

while the moving 1/tanh solution (inverted kink) is

$$\psi_n(t) = \frac{A\,\mathrm{e}^{\mathrm{i}(\omega t + \alpha n + \phi_0)}}{\tanh[\beta h(n + x_0 - vt)]}, \tag{37}$$

and it has the same parameters as the solution of equation (36).

The parameter α in the moving solutions is related to the propagation velocity v and it depends on the model parameters δ_i. For fixed δ_i, the moving solution exists only for an isolated propagation velocity. However, for $\delta_1 = \delta_3 = 0$, which is the case of the integrable lattice, one can take arbitrary $-\pi \leqslant \alpha \leqslant \pi$ and hence, the velocity can change continuously.

Since $|\cos\alpha| \leqslant 1$, the moving solutions are defined not in the whole parameter plane presented in figure 1, but only for $|\delta_1/\delta_3| = |\delta_1/(1-\delta_1-\delta_2)| \leqslant 2$.

We also note that the amplitude of the moving solutions diverges at $\delta_2 = \delta_3$ and one has to set one more constraint on the parameters for existence of these solutions, namely $\delta_2 \neq (1-\delta_1)/2$. On this line, the norm N is conserved and we thus conclude that the norm-conserving subclass of equation (10) does not admit moving solutions.

6. Stability analysis

6.1. Numerical method

Let us now study the stability of the stationary solution equation (9). Following the methodology of reference [20], we consider the following perturbed form of the solutions,

$$\psi_n(t) = [f_n + \epsilon_n(t)]\,\mathrm{e}^{\mathrm{i}\omega t}, \tag{38}$$

where the small complex perturbation $\epsilon_n(t)$ is expressed as follows:

$$\epsilon_n(t) = a(t) + \mathrm{i}b(t). \tag{39}$$

Substituting equation (38) into equation (10) we find that $\epsilon_n(t)$ is governed by the following linearized equation:

$$\begin{aligned}\mathrm{i}\dot{\epsilon}_n - \omega\epsilon_n + \frac{1}{2h^2}(\epsilon_- - 2\epsilon_n + \epsilon_+) + \delta_1\frac{\lambda}{2}\big[f_n^2(a_- + a_+) + f_n(f_- + f_+)(a_n + \epsilon_n)\big] \\ + \delta_2\frac{\lambda}{2}\big[2f_n(f_- + f_+)a_n + f_n^2(\epsilon_- + \epsilon_+)\big] \\ + \delta_3\frac{\lambda}{2}\big[f_n^2(\epsilon_-^* + \epsilon_+^*) + 2f_n(f_- + f_+)\epsilon_n\big] = 0.\end{aligned} \tag{40}$$

Then, separating real and imaginary parts of equation (40) we derive the following system:

$$\begin{pmatrix}\dot{\mathbf{b}}\\ \dot{\mathbf{a}}\end{pmatrix} = \begin{pmatrix}0 & \mathbf{K}\\ \mathbf{J} & 0\end{pmatrix}\begin{pmatrix}\mathbf{b}\\ \mathbf{a}\end{pmatrix}, \tag{41}$$

where vectors $\mathbf{a}$ and $\mathbf{b}$ contain a_n and b_n, respectively, while the nonzero coefficients of matrices $\mathbf{K}$ and $\mathbf{J}$ are given by

$$\begin{aligned} K_{n,n} &= -\frac{\Omega}{h^2} + \lambda f_n(f_- + f_+), & K_{n,-} = K_{n,+} &= \frac{1}{2h^2} + \frac{\lambda}{2}f_n^2,\\ J_{n,n} &= \frac{\Omega}{h^2} - \frac{\lambda}{2}(\delta_1 + 2\delta_3)f_n(f_- + f_+), & J_{n,-} = J_{n,+} &= -\frac{1}{2h^2} - \frac{\lambda}{2}(\delta_2 - \delta_3)f_n^2. \end{aligned} \tag{42}$$

In the above expressions, $n = 1, \ldots, \mathcal{N}$, where $\mathcal{N}$ is the number of particles of the chain. For symmetric solutions, periodic boundary conditions are imposed. For the localized hyperbolic function solutions that shift the phase by π, e.g., for the tanh solution equation (55) and 1/tanh solution equation (56), the anti-periodic boundary conditions were used. In this case, we change the signs of the following elements $K_{1,\mathcal{N}} = -\frac{1}{2h^2} - \frac{\lambda}{2}f_1^2$, $K_{\mathcal{N},1} = -\frac{1}{2h^2} - \frac{\lambda}{2}f_{\mathcal{N}}^2$, and, similarly, $J_{1,\mathcal{N}} = \frac{1}{2h^2} + \frac{\lambda}{2}(\delta_2 - \delta_3)f_1^2$, $J_{\mathcal{N},1} = \frac{1}{2h^2} + \frac{\lambda}{2}(\delta_2 - \delta_3)f_{\mathcal{N}}^2$. On the other hand, if, e.g., a kink–antikink pair is considered, then the total phase shift is zero and the normal periodic

boundary conditions can again be used. A stationary solution is characterized as linearly stable if and only if the eigenvalue problem

$$\begin{pmatrix} 0 & \mathbf{K} \\ \mathbf{J} & 0 \end{pmatrix} \begin{pmatrix} \mathbf{b} \\ \mathbf{a} \end{pmatrix} = \gamma \begin{pmatrix} \mathbf{b} \\ \mathbf{a} \end{pmatrix} \tag{43}$$

results in nonpositive real parts of all eigenvalues γ.

For the TI lattices discussed in the present study, the eigenvalue problem equation (43) always gives rise to two pairs of zero γ, one pair corresponding to the invariance with respect to translation, and another pair to the invariance with respect to the rotation/phase shift. These eigenmodes are derived below.

6.2. Phase invariant and translationally invariant eigenvectors

Phase invariance of equation (10) means that arbitrary phase shift $\Delta\phi$ can be applied to a stationary solution of the form $\psi_n = f_n \, \mathrm{e}^{\mathrm{i}(\omega t + \Delta\phi)}$. For small $\Delta\phi$, the latter expression can be approximated as

$$\psi_n = (f_n + \mathrm{i} f_n \Delta\phi) \, \mathrm{e}^{\mathrm{i}\omega t}, \tag{44}$$

which should be compared to equation (38), revealing the generator of the group associated with the invariance. The following eigen-pair

$$\gamma = 0, \qquad \begin{pmatrix} \mathbf{b} \\ \mathbf{a} \end{pmatrix} = k \begin{pmatrix} \mathbf{f} \\ \mathbf{0} \end{pmatrix} \tag{45}$$

(with k being the normalizing factor) satisfies the eigenvalue problem equation (43). Indeed, substituting equation (45) into equation (43) we obtain $\mathbf{Jf} = \mathbf{0}$ or, in the explicit form $J_{n,-} f_- + J_{n,n} f_n + J_{n,+} f_+ = 0$. Utilizing equation (42), the last expression reduces to equation (7), which is satisfied for the considered stationary solution. Thus, for the stationary solution satisfying equation (7), the eigenvalue problem equation (43) is satisfied by the eigen-pair equation (45).

Similarly, one can find the translationally invariant eigenvector. In the TI lattices, the stationary solutions have the form $\psi_n = f_n[\beta h(n + x_0)] \, \mathrm{e}^{\mathrm{i}\omega t}$ with arbitrary shift x_0. Let us consider a small increment of the shift, Δx_0, and expand the solution taking into account only the linear term. This way we obtain

$$\psi_n = (f_n + \beta h f_n' \Delta x_0) \, \mathrm{e}^{\mathrm{i}\omega t}, \tag{46}$$

where f_n' denotes the derivative of f_n with respect to its argument. Comparing this with equation (38) one can see that the translational eigen-pair should be as follows:

$$\gamma = 0, \qquad \begin{pmatrix} \mathbf{b} \\ \mathbf{a} \end{pmatrix} = k \begin{pmatrix} \mathbf{0} \\ \mathbf{f}' \end{pmatrix}. \tag{47}$$

To confirm that, we substitute equation (47) into equation (43) and obtain $\mathbf{Kf}' = \mathbf{0}$, or $K_{n,-} f_-' + K_{n,n} f_n' + K_{n,+} f_+' = 0$. The last expression, with the use of equation (42), transforms to

$$\frac{1}{2h^2}(f_-' - 2f_n' + f_+') - \omega f_n' + \frac{\lambda}{2} f_n^2 (f_-' + f_+') + \lambda(f_- + f_+) f_n f_n' = 0, \tag{48}$$

which is proportional to the derivative of equation (7) with respect to x_0. Since equation (7) is identically satisfied for the considered stationary solution for arbitrary x_0, it can be differentiated yielding equation (48). Thus, for the stationary solutions satisfying equation (7), the eigenvalue problem equation (43) is satisfied by the translationally invariant eigen-pair

equation (47). Note that derivation of equation (7) with respect to x_0 is meaningful only for the TI models.

One can boost a stationary solution along the translationally invariant mode. We first note that while the eigenvalue problem $\mathbf{Kf}' = \mathbf{0}$ has a single root $\gamma = 0$, the extended problem equation (43) has $\gamma^2 = 0$ corresponding to a pair of the eigenvalues associated with translational invariance. Then, we write the following solution to the real and imaginary parts of equation (40), employing the eigenvector equation (47),

$$\begin{pmatrix} b_n(t) \\ a_n(t) \end{pmatrix} = v \begin{pmatrix} \mathbf{0} \\ (1+t)\mathbf{f}' \end{pmatrix}. \tag{49}$$

Substituting equation (49) into equation (38) we obtain an approximate *moving* solution to the nonlinear equation (10), whose accuracy increases with decrease in the eigenmode amplitude v, which is proportional (for small v) to the propagation velocity.

6.3. Stability of the plane-wave solution

We consider the simplest plane-wave solution of the form

$$\psi_n(t) = \pm A\, \mathrm{e}^{\mathrm{i}\omega t}, \qquad A = \sqrt{\frac{\omega}{\lambda}} = \frac{\sqrt{1-\Omega}}{h}, \tag{50}$$

where the real amplitude A is found upon substituting the solution into equation (10). We are interested in the (modulational) stability of this solution for the following reasons: First, this solution is in fact the dn solution equation (31) in the limit $m \to 1$. Second, the above plane-wave solution is in fact the background of the tanh, equation (55), and 1/tanh, equation (56), solutions (see the asymptotic limits of equations (55) and (56) for $|n| \to \infty$). Naturally, the latter two solutions cannot be stable if their 'pedestal', i.e., the plane-wave solution of equation (50), is modulationally unstable.

Setting $f_n = A$ in equation (42) we then present equation (41) as a system of second-order linear differential equations $\ddot{\mathbf{a}} = \mathbf{JKa}$. Seeking for small-amplitude wave solutions of the form $a_n(t) \sim \exp(\mathrm{i}Qhn - \mathrm{i}\Gamma t)$, characterized by a frequency Γ and a wavenumber Q, we derive the following dispersion relation:

$$\Gamma^2(Q) = 4\left[-\frac{1}{h^2} + \lambda(1-\delta_1-2\delta_2)A^2\right]\left[\lambda A^2 - \left(\frac{1}{h^2} + \lambda A^2\right)\sin^2\left(\frac{Qh}{2}\right)\right]\sin^2\left(\frac{Qh}{2}\right). \tag{51}$$

Each positive (negative) Γ^2 gives two purely imaginary (real) eigenvalues of the original problem equation (43), $\gamma_i = \pm\mathrm{i}\sqrt{\Gamma^2}$ ($\gamma_r = \pm\sqrt{-\Gamma^2}$).

The solution equation (50) is modulationally stable for wavenumbers Q such that $\Gamma^2(Q) > 0$.

For $\lambda = 1$, equation (51) always has regions of Q with negative Γ^2, which indicates the instability of the plane-wave solution of equation (50).

For $\lambda = -1$ the stability condition is

$$\frac{1}{h^2} + (1-\delta_1-2\delta_2)A^2 \geqslant 0. \tag{52}$$

This condition can be satisfied at any point of the model parameter space (δ_1, δ_2) shown in figure 1, if the amplitude A or/and the lattice spacing h are sufficiently small. On the other hand, in the region of the parameter space with $\delta_1 + 2\delta_2 \leqslant 1$, the stability condition is satisfied for any A and h.

Setting $A = 0$ in equation (51) we obtain the spectrum of the vacuum ($\psi_n = 0$),

$$\Gamma^2 = \frac{4}{h^4}\sin^4\left(\frac{Qh}{2}\right), \tag{53}$$

which is always stable.

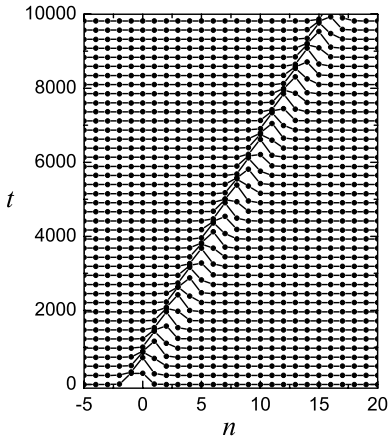

Figure 4. Space-time evolution of $|\psi_n(t)|^2$ showing slow motion of the pulse, equation (54), in the non-integrable, TI lattice. The moving highly localized pulse does not produce any noticeable radiation. Parameters: $\lambda = 1$, $\delta_1 = \delta_2 = \delta_3 = 1/3$, $h = 2$, $\Omega = 3$, $\omega = 0.5$.

To conclude, the plane-wave solution equation (50) with $A > 0$ is stable for $\lambda = -1$ if equation (52) is satisfied. The solution is stable with respect to small-amplitude sinusoidal waves with any wavenumber Q. For $\lambda = 1$ and $A > 0$, there are always unstable modes with $Q > 0$. The vacuum solution ($A = 0$) is stable.

6.4. Pulse solution (bright soliton)

The cn and dn solutions ($\lambda = 1$) described in section 4.2, in the limit of $m \to 1$, reduce to the pulse solution

$$f_n = \pm A \,\mathrm{sech}[\beta h(n + x_0)],$$
$$\Omega = \cosh(\beta h), \qquad A = \frac{\sqrt{\Omega^2 - 1}}{h}, \qquad S = 0. \tag{54}$$

For the stationary pulse in a chain of $\mathcal{N} = 200$ sites we calculate the spectrum of small-amplitude vibrations solving numerically the eigenvalue problem equation (43). The pulse solution was found to be stable in a wide range of the model parameters δ_i, the discreteness parameter h, and the pulse frequency ω.

As an example, figure 4 illustrates a highly localized pulse propagating at slow speed of $v = 0.017$ in the non-integrable, TI lattice with $\delta_1 = \delta_2 = \delta_3 = 1/3$. The lattice spacing is $h = 2$ and the pulse frequency is $\omega = 0.5$. The moving pulse does not produce any noticeable radiation. A zero-frequency normalized translational mode with a small amplitude was used to boost the pulse, as described in section 6.2. According to equations (47) and (54), the translational eigenmode is $b_n = 0$, $a_n \sim f_n' \sim \mathrm{sech}[\beta h(n + x_0)] \tanh[\beta h(n + x_0)]$.

For the considered parameters, we did not observe in the spectrum of the stationary pulse any localized modes except for the four zero-frequency modes. The rest of eigenvalues appear in the phonon band ranging from ω to $\omega + \Gamma_{\max}$ with $\Gamma_{\max} = 2/h^2$ (see equation (53) for $Q = \pi/h$).

6.5. Kink solution (dark soliton)

In the limit of $m \to 1$, the sn solution ($\lambda = -1$) described in section 4.2 reduces to the kink solution

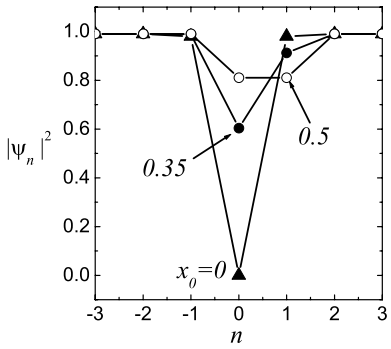

Figure 5. Kink (dark soliton) profiles for $x_0 = 0, 0.35$ and 0.5 at $\lambda = -1$, $h = 1$, $\Omega = 0.01$, $\omega = -0.99$. Stationary kink profiles do not depend on the parameters δ_i. The degree of kink localization increases as positive Ω approaches zero.

$$f_n = \pm A \tanh[\beta h(n + x_0)],$$
$$\Omega = \operatorname{sech}^2(\beta h), \qquad A = \frac{\sqrt{1-\Omega}}{h}, \qquad S = -h^2 A^4. \tag{55}$$

In standard DNLS models dark solitons typically survive the anti-continuum limit ($h \to \infty$) [21, 22], but in the present model they do not. Indeed, the iterative formula equation (25), for $\lambda = -1$ and $S = -h^2A^4 = -h^2\omega^2$, reduces to $f_n = -\omega/f_-$ with the zigzag solution $f_{2n} = f_0$, $f_{2n+1} = -\omega/f_0$, which is not a dark soliton. This qualitative difference is due to the fact that, in the models discussed here, coupling between nearest neighbours takes place also in the anharmonic term and it remains in the system even if the harmonic coupling terms are neglected.

On the other hand, highly localized dark solitons can be observed in the discussed DNLS models at finite h when the inverse kink width βh is very large, which happens for small positive Ω (see the first expression in the second line of equation (55)).

Robust dark solitons were found on the line $\delta_1 = 0$ (see figure 1). These structures will be discussed in this case and in the highly localized regimes, $\Omega = 0.1$ and 0.01. For the lattice spacing we set $h = 1$.

For these parameters we find from equation (52) that the plane-wave structure carrying the kink solution becomes unstable for $\delta_2 > (1 - \Omega/2)/(1 - \Omega)$. Taking $\Omega = 0.01$ we find $\delta_2 > 1.005$, i.e., the highly localized kink becomes unstable slightly above the integrable case ($\delta_2 = 1$).

The equilibrium kink profile does not depend on δ_i; examples of kinks for several values of x_0 and $\Omega = 0.01$ are shown in figure 5 to demonstrate that, for chosen parameters, the kink is highly localized.

For the kink in a chain of $\mathcal{N} = 200$ sites we calculate the spectrum of small-amplitude vibrations solving numerically the eigenvalue problem equation (43). As an example, in figure 6 we show the spectrum of the on-site kink ($x_0 = 0$) shown in figure 5 for $\delta_1 = 0$ and different values of δ_2 decreasing from (a)–(d) as indicated in each panel. As noted above, the plane wave carrying the kink is unstable for $\delta_2 > 1.005$, as can be seen in (a). The kink is stable for $\delta_2 < 1.005$ (see in (b)–(d)). For $1.0 < \delta_2 < 1.005$ the stable kink possesses a localized vibrational mode which enters the phonon band at $\delta_2 = 1$, corresponding to the integrable case. The phonon band of the kink is given by equation (51) and it has $\Gamma_{\max} = (2/h^2)\sqrt{1 + (1 - \delta_1 - 2\delta_2)(1 - \Omega)}$. The spectrum of the inter-site kink is similar.

The robustness of the moving kinks is demonstrated in figure 7 by simulating their collision. Here we take $\Omega = 0.1$, while other parameters are unchanged. One can see

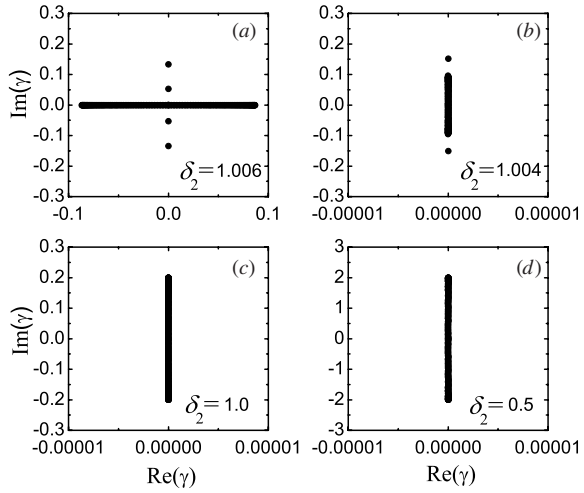

Figure 6. Spectrum of the on-site kink ($x_0 = 0$) shown in figure 5 for $\delta_1 = 0$ and different values of δ_2 decreasing from (*a*) to (*d*) as indicated in each panel. The plane wave carrying the kink is unstable for $\delta_2 > 1.005$, as can be seen in (*a*). The kink is stable for $\delta_2 < 1.005$ (see (*b*) to (*d*)). For $1.0 < \delta_2 < 1.005$ the stable kink possesses a localized vibrational mode which enters the phonon band at $\delta_2 = 1$, corresponding to the integrable case. The spectrum of the inter-site kink is similar. We found also that kinks in the TI model presented here can be stable in the weakly localized regime, which contrasts to the behaviour of kinks in the generic discrete models [21, 22].

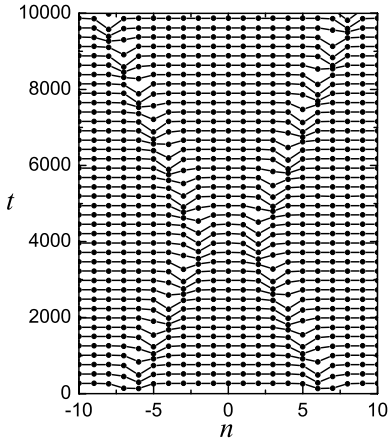

Figure 7. Space-time evolution of $|\psi_n(t)|^2$ showing practically elastic collision of two highly localized, slowly moving dark solitons (kinks) in the non-integrable TI lattice. Parameters: $\lambda = -1$, $h = 1, \delta_1 = 0, \delta_2 = \delta_3 = 0.5, \Omega = 0.1, \omega = -0.9$.

that the collision of highly localized kinks is practically elastic and without any noticeable radiation. To boost the kinks we used the translational eigenmode with a small amplitude, as described in section 6.2. As follows from equations (47) and (55), the translational eigenmode is $b_n = 0, a_n \sim f_n' \sim \mathrm{sech}^2[\beta h(n + x_0)]$.

In the classical DNLS equation, only highly localized on-site dark solitons close to the anti-continuum limit are stable, while inter-site ones are unstable at any degree of discreteness [21, 22]. In the TI model discussed here we found that they can be stable also in a weakly localized regime and at any position with respect to the lattice. The principal reason is

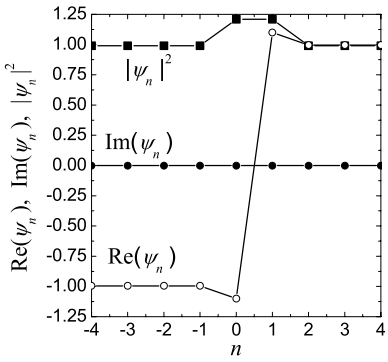

Figure 8. Inter-site inverted kink profile in the highly localized regime. Parameters: $\lambda = -1$, $h = 1, \Omega = 0.01, \omega = -0.99, x_0 = 0.5$. Profile of the stationary inverted kink does not depend on the parameters δ_i.

that the instability is driven by the bifurcation of the eigenvalues associated with translation. In the present class of models, since TI is restored and the relevant eigenvalue is at the origin of the spectral plane, the (oscillatory) instabilities of discrete dark solitons are no longer present. This is one of the critical differences between TI and generic discrete models in this context.

6.6. Inverted kink solution

In the limit of $m \to 1$, the 1/sn solution ($\lambda = -1$) presented in section 4.2 reduces to the inverted kink solution

$$f_n = \frac{\pm A}{\tanh[\beta h(n + x_0)]}, \tag{56}$$

with the parameters Ω, A and S being the same as for the tanh solution, equation (55).

To obtain a highly localized inverted kink we take the following parameters, $\lambda = -1$, $h = 1$, $\Omega = 0.01$, $\omega = -0.99$ (same as we took for the kink).

The inter-site inverted kink is shown in figure 8 and its profile does not depend on δ_i.

For the stationary inverted kink in a chain of $\mathcal{N} = 200$ sites we calculate the spectrum of small-amplitude vibrations solving numerically the eigenvalue problem equation (43) and show several results in figure 9 for $\delta_1 = 0$ and different values of the parameter δ_2.

For the chosen parameters, the inter-site inverted kink ($x_0 = 0.5$) was found to be stable on the line $\delta_1 = 0$ within the range of $0.897 < \delta_2 < 1.0045$, while the asymmetric inverted kink at $x_0 = 0.4$ within a somewhat narrower range of $0.915 < \delta_2 < 1.0043$. These intervals include the integrable lattice with $\delta_2 = 1$. As it was mentioned in the discussion of the kink, for the chosen parameters, the plane-wave structure carrying the inverted kink becomes unstable for $\delta_2 > 1.005$.

The spectrum of the inverted kink for $\delta_2 \leqslant 1$ consists of the phonon band, equation (51), and the four zero eigenvalues. For $\delta_2 > 1$ a pair of purely imaginary eigenvalues lying outside of the phonon band can be observed, as can be seen in figures 9(*a*) and (*b*). This is the sign of the appearance of a vibrational mode localized around the inverted kink.

7. Exact moving solutions to the continuum NLS equation

In the continuum limit, $h \to 0$, the borders of the admissible region, equation (23), become

$$\left(f_0^2\right)_{1,2} = \frac{\omega}{\lambda} \pm \sqrt{\left(\frac{\omega}{\lambda}\right)^2 - \frac{C}{\lambda}}. \tag{57}$$

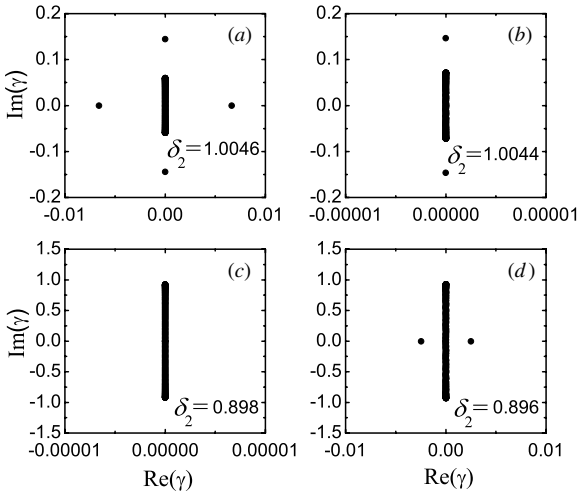

Figure 9. Spectrum of the inter-site inverted kink ($x_0 = 0.5$) shown in figure 8 for $\delta_1 = 0$ and different values of δ_2 decreasing from (*a*) to (*d*) as indicated in each panel. The plane wave carrying the inverted kink is unstable for $\delta_2 > 1.005$. The inverted kink is stable within the window $0.897 < \delta_2 < 1.0045$ and panel (*a*) shows the spectrum slightly above, while panel (*d*) slightly below the stability window. For comparison, panels (*b*) and (*c*) show the spectrum within the stability window close to the upper and to the lower edges, respectively. For $\delta_2 > 1$ the inverted kink possesses a localized vibrational mode (see in (*a*) and (*b*)), which enters the phonon band at $\delta_2 = 1$, corresponding to the integrable case.

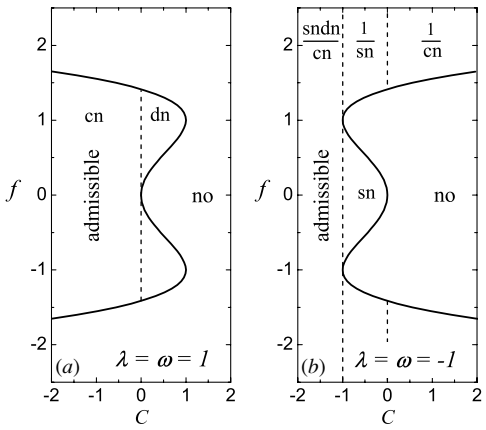

Figure 10. Admissible regions for the continuum DNLS equation, equation (1), for (*a*) $\lambda = +1$ and (*b*) $\lambda = -1$ obtained as the continuum limits ($h \to 0$) of those presented in figures 2 and 3, respectively. In each panel there is one inadmissible region marked with 'no'.

In figure 10 we plot the admissible regions for (*a*) $\lambda = \omega = 1$ and (*b*) $\lambda = \omega = -1$. The topology of the admissible regions for the continuum NLS equation is simpler than the one pertaining to the discrete models. In the continuum limit there exists a sole inadmissible region for both cases $\lambda = \pm 1$, while three inadmissible regions exist for the discrete models in the case $\Lambda < 0$. One more simplification is that the domains of the sndn/cn and cn solutions do not split into two parts since the smaller root β_1 disappears in the continuum limit. Particularly we note that the region marked with the question mark in figure 3 disappears in the continuum limit.

The static solutions equations (29)–(34) obtained for the discrete model equation (10) have their continuum counterparts as the travelling solutions to the NLS field, equation (1). The general form of the solutions is

$$\begin{aligned} &\psi(x,t) = \pm A\,\mathrm{sn}^q(z,m)\,\mathrm{cn}^r(z,m)\,\mathrm{dn}^s(z,m)\exp(y),\\ &msz = \beta(x + x_0 - vt),\\ &y = \mathrm{i}(vx + \omega t + \phi_0), \end{aligned} \tag{58}$$

where $0 \leqslant m \leqslant 1$ is the modulus of the Jacobi elliptic functions, A, β, v and ω are the parameters of the solution, x_0 and ϕ_0 are the arbitrary initial position and phase, respectively. The integers q, r, s once again specify the particular form of the solution.

The continuum analogues of equations (29)–(34) have the following form and are characterized by the respective relations between parameters.

The sn solution, $(q, r, s) = (1, 0, 0)$,

$$\begin{aligned} &2\omega = -\beta^2(m+1) - v^2, \qquad A = \beta\sqrt{-\frac{m}{\lambda}},\\ &C = \frac{\lambda}{m}A^4, \qquad \frac{\omega^2}{\lambda} < C < 0. \end{aligned} \tag{59}$$

The cn solution, $(q, r, s) = (0, 1, 0)$,

$$\begin{aligned} &2\omega = \beta^2(2m-1) - v^2, \qquad A = \beta\sqrt{\frac{m}{\lambda}},\\ &C = \frac{\lambda}{m}(m-1)A^4, \qquad -\infty < C < 0. \end{aligned} \tag{60}$$

The dn solution, $(q, r, s) = (0, 0, 1)$,

$$\begin{aligned} &2\omega = \beta^2(2-m) - v^2, \qquad A = \beta\sqrt{\frac{1}{\lambda}},\\ &C = (1-m)\lambda A^4, \qquad 0 < C < \frac{\omega^2}{\lambda}. \end{aligned} \tag{61}$$

The 1/sn solution, $(q, r, s) = (-1, 0, 0)$,

$$\begin{aligned} &2\omega = -\beta^2(1+m) - v^2, \qquad A = \beta\sqrt{-\frac{1}{\lambda}},\\ &C = m\lambda A^4, \qquad \frac{\omega^2}{\lambda} < C < 0. \end{aligned} \tag{62}$$

The 1/cn solution, $(q, r, s) = (0, -1, 0)$,

$$\begin{aligned} &2\omega = \beta^2(2m-1) - v^2, \qquad A = \beta\sqrt{\frac{m-1}{\lambda}},\\ &C = \frac{m\lambda}{m-1}A^4, \qquad 0 < C < \infty. \end{aligned} \tag{63}$$

The sndn/cn solution, $(q, r, s) = (1, -1, 1)$,

$$\begin{aligned} &2\omega = -2\beta^2(2m-1) - v^2, \qquad A = \beta\sqrt{-\frac{1}{\lambda}},\\ &C = \lambda A^4, \qquad -\infty < C < \frac{\omega^2}{\lambda}. \end{aligned} \tag{64}$$

The above six solutions can be rewritten in many other forms using the properties of the Jacobi elliptic functions [23]. However, we believe that they span the entire two-parameter

space, (C, f) of standing wave solutions, obtained as the continuum limit of corresponding space of the discrete models.

All solutions are conveniently parameterized by a single parameter $-\infty < C < \omega^2/\lambda$ for $\lambda > 0$, and $-\infty < C < \infty$ for $\lambda < 0$, as it is presented in figure 10.

The solutions in equations (59)–(61) are bounded while the other ones are unbounded. The solutions in equations (60) and (61) are defined for $\lambda > 0$ while the others for $\lambda < 0$.

8. Conclusions

Our main findings for the two-parameter TI DNLS model equation (10) can be summarized as follows:

- Subclasses of the model conserving quantities equations (14)–(16) have been found in section 3 (see figure 1).
- All stationary solutions of the form of equation (9) can be found from the DFI equation (6), which is a quadratic equation with the solution of equation (21). The whole set of solutions is parameterized by the integration constant C entering the DFI and the initial value f_0. Admissible values of f_0 for given C are presented in figures 2 and 3 for $\lambda = 1$ and $\lambda = -1$, respectively.
- Many of the existing stationary solutions were expressed in terms of the Jacobi elliptic functions. The general form of the solutions is given by equation (26) and the parameters of particular solutions are displayed in equations (29)–(34). The Jacobi elliptic function solutions were related to that in the form of the quadratic map (see figures 2 and 3). In the portion of figure 3 marked with the question mark the Jacobi elliptic function solution of the form of equation (26) was not found. We speculate that the reason of failure is that this region disappears in the continuum limit.
- Exact moving solutions to equation (10) in the form of the hyperbolic functions are given by equations (35)–(37) and similar solutions in the form of the Jacobi elliptic functions can also be obtained. For fixed model parameters δ_i there exists an isolated propagation velocity. However, for $\delta_1 = \delta_3 = 0$, which corresponds to the integrable lattice, the propagation velocity can change continuously.
- The spectrum of small-amplitude vibrations in the vicinity of the stationary solutions was investigated. For the TI models the spectrum always contains two pairs of zero eigenvalues, one pair corresponds to the translational invariance and another pair to the invariance with respect to the phase shift. Phase invariant and translationally invariant eigen-pairs are given by equations (45) and (47), respectively. Stationary solutions can be set in slow motion with the use of the translationally invariant eigenvector as described in section 6.2.
- Examples of stable pulses (bright solitons), kinks (dark solitons) and inverted kinks are given in sections 6.4–6.6. Bright and dark solitons propagating at slow speed do not radiate energy because the translational eigenmode used for boosting is a solution to the linearized equation whose accuracy grows for decreasing eigenmode amplitude, i.e., with decrease in propagation velocity. A key difference between TI models and their generic DNLS discretization counterparts [21, 22] can be found in the parameter range of stability of the dark solitons which is much narrower in the latter; dark solitons are practically always stable in the former, provided that their background is (modulationally) stable.
- A complete set of standing wave solutions to the continuum NLS equation with focusing/defocusing Kerr nonlinearity, equation (1), is presented by equations (59)–(64).

These solutions fill the whole admissible region obtained as the continuum limit of the regions found for the discrete models.

Our study opens a number of new problems and research directions. Particularly, it would be interesting to investigate whether the Jacobi elliptic function solutions can be obtained for DFIs of higher order. It would also be of interest to systematically examine the stability in such discrete systems of the full elliptic function solutions, also as a function of their elliptic modulus. Furthermore, from a mathematical perspective, it would be worthwhile to examine the well posedness of these models, especially in the case of the non-norm preserving settings (when N is conserved, it can be straightforwardly used to infer global existence of the solution in time). Finally, generalizing such approaches to higher dimensions and attempting to obtain analytical solutions in the latter context would constitute another very timely direction for future work.

Acknowledgments

PGK gratefully acknowledges the support of NSF-DMS-0204585, NSF-DMS-0505063 and NSF-CAREER.

References

[1] Ablowitz M J and Ladik J F 1975 Nonlinear differential-difference equations *J. Math. Phys.* **16** 598–6
Ablowitz M J and Ladik J F 1976 Nonlinear differential-difference equations and Fourier analysis *J. Math. Phys.* **17** 1011–8
[2] Toda M 1981 *Theory of Nonlinear Lattices* (Berlin: Springer)
[3] Orfanidis S J 1978 Sine-Gordon equation and nonlinear σ model on a lattice *Phys. Rev.* D **18** 3828–5
[4] Speight J M and Ward R S 1994 Kink dynamics in a novel discrete sine-Gordon system *Nonlinearity* **7** 475–11
[5] Speight J M 1999 Topological discrete kinks *Nonlinearity* **12** 1373–17
[6] Kevrekidis P G 2003 On a class of discretizations of Hamiltonian nonlinear partial differential equations *Physica* D **183** 68–19
[7] Dmitriev S V, Kevrekidis P G and Yoshikawa N 2005 Discrete Klein–Gordon models with static kinks free of the Peierls-Nabarro potential *J. Phys. A: Math. Gen.* **38** 7617–11
[8] Dmitriev S V, Kevrekidis P G, Yoshikawa N and Frantzeskakis D J 2006 Exact static solutions for discrete ϕ^4 models free of the Peierls-Nabarro barrier: discretized first integral approach *Phys. Rev.* E **74** 046609-15
[9] Barashenkov I V, Oxtoby O F and Pelinovsky D E 2005 Translationally invariant discrete kinks from one-dimensional maps *Phys. Rev.* E **72** 035602–4
[10] Oxtoby O F, Pelinovsky D E and Barashenkov I V 2006 Travelling kinks in discrete ϕ^4 models *Nonlinearity* **19** 217–19
[11] Cooper F, Khare A, Mihaila B and Saxena A 2005 Exact solitary wave solutions for a discrete $\lambda\phi^4$ field theory in 1 + 1 dimensions *Phys. Rev.* E **72** 36605–11
[12] Speight J M and Zolotaryuk Y 2006 Kinks in dipole chains *Nonlinearity* **19** 1365–18
[13] Dmitriev S V, Kevrekidis P G and Yoshikawa N 2006 Standard nearest-neighbour discretizations of Klein–Gordon models cannot preserve both energy and linear momentum *J. Phys. A: Math. Gen.* **39** 7217–10
[14] Roy I, Dmitriev S V, Kevrekidis P G and Saxena A 2006 Comparative study of different discretizations of the ϕ^4 model *Preprint* nlin.PS/0608046
[15] Kevrekidis P G, Dmitriev S V and Sukhorukov A A 2006 On a class of spatial discretizations of equations of the nonlinear Schrödinger type *Math. Comput. Simulat.* at press (DOI:10.1016) (*Preprint* j.matcom.2006.10.014)
Kevrekidis P G, Dmitriev S V and Sukhorukov A A 2006 *Preprint* nlin.SI/0603046
[16] Dmitriev S V, Kevrekidis P G, Sukhorukov A A, Yoshikawa N and Takeno S 2006 Discrete nonlinear Schrödinger equations free of the Peierls–Nabarro potential *Phys. Lett.* A **356** 324–9 (see also *Preprint* nlin.PS/0603047 with corrected misprints)
[17] Khare A, Rasmussen K, Samuelsen M R and Saxena A 2005 Exact solutions of the saturable discrete nonlinear Schrödinger equation *J. Phys. A: Math. Gen.* **38** 807–8
[18] Khare A, Rasmussen K, Salerno M, Samuelsen M R and Saxena A 2006 Discrete nonlinear Schrödinger equations with arbitrarily high-order nonlinearities *Phys. Rev.* E **74** 016607–11

[19] Pelinovsky D E 2006 Translationally invariant nonlinear Schrödinger lattices *Nonlinearity* **19** 2695–716
[20] Carr J and Eilbeck J C 1985 *Phys. Lett.* A **109** 201
[21] Fitrakis E P, Kevrekidis P G, Susanto H and Frantzeskakis D J 2006 Dark solitons in discrete lattices: saturable versus cubic nonlinearities *Preprint* nlin.PS/0608023
[22] Johansson M and Kivshar Yu S 1999 Discreteness-induced oscillatory instabilities of dark solitons *Phys. Rev. Lett.* **82** 85–4
[23] *Handbook of Mathematical Functions* 1964 ed M Abramowitz and I A Stegun (Washington, DC: US Govt Printing Office)